
Open Archive TOULOUSE Archive Ouverte (OATAO)
OATAO is an open access repository that collects the work of Toulouse researchers and makes it freely available over the web where possible.

This is an author-deposited version published in : http://oatao.univ-toulouse.fr/
Eprints ID : 12012

**To link to this article** : DOI:10.1007/s00170-014-6217-5
http://dx.doi.org/10.1007/s00170-014-6217-5

**To cite this version :** Wagner, Vincent and Duc, Emmanuel *Study of Ti-1023 milling with toroidal tool.* (2014) The International Journal of Advanced Manufacturing Technology . ISSN 0268-3768

Any correspondance concerning this service should be sent to the repository administrator: staff-oatao@listes-diff.inp-toulouse.fr

# Study of Ti-1023 milling with toroidal tool

**Vincent Wagner · Emmanuel Duc**

**Abstract** The Ti-1023 beta alloy titanium is used in aeronautics for the production of structure parts such as landing gear and as most of titanium alloys its machinability is poor explained by its physical and mechanical properties. This work presents the machinability results carried out for Ti-1023 milling in using toroidal tool. The aim of this research is the understanding of tool wear mechanisms and to establish the relation between cutting conditions, milling tool geometry, and tool life. A section is also devoted to the chip analysis. The wear modes are also analyzed and defined for different cutting tool geometries where several steps occur. This study is focus on material removal rate, tool life, and volume.

**Keywords** Ti-1023 · Milling · Tool wear · Cutting conditions · Toroidal tool

## 1 Introduction

For many years, machining of titanium alloys has became a very important problematic in the aeronautical industry. This difficulty is related to the low machinability of titanium alloys but also to their diversity. In recent years, many alloys of titanium (Ti-64, Ti-1023, Ti-5553, Ti-17...) have emerged and often with a low machinability. This machinability is due to high strengths, high cutting temperatures, and a high chemical reactivity with the most of cutting tool materials [1]. Wagner compares the mechanical and the physical properties of Ti-64 and Ti-5553 [2]. Identical physical behavior for both materials but a large difference in mechanical behavior has been noted and may explain the poor machinability. For example, the Ti-5553 titanium alloy, its low machinability is mainly due to its concentration in alphagene elements [3]. Concerning the Ti-64, some studies show also its low machinability. However, few studies concern the machinability of Ti-1023 titanium alloy. But its chemical composition compared to the common titanium alloys as the Ti-64 can induce a difference. Machai notes that a slower cutting speed ($V_c < 50\,m/min$) is recommended in order to avoid catastrophic failure [4]. For higher cutting speeds ($V_c > 100\,m/min$), the flank wear increases rapidly.

The toroidal cutter can be used in many sort of operations : contouring and surfacing. Its cylindrical inserts allow also milling of complex surfacing. Moreover, compared to a cylindrical tool with a constant cutting engagement, the high cutting edge angle reduces the chip cross section and consequently decreases the cutting forces. An highest tool life could be then expected. In addition to increase the productivity, a new tool cutter positioning can be used [5]. The considered tool inclination is towards the back of the tool. In this case, all inserts work simultaneously and generate a continuous cutting phenomenon.

However, the advantages of toroidal tool used in machining of titanium alloys are not yet demonstrated and their use can be optimized. This work presents a study of the employment of toroidal tool during the Ti-1023 milling. In first section, an optimal range of cutting conditions in using the French method of Tool Material Couple (COM) is defined [6]. A part of this study, will be devoted to the study of the chip formation with torus tool. The last section presents a

V. Wagner (✉)
Université de Toulouse INP/ENIT, LGP, 47 avenue d'Azereix, BP 1629, 65013 Tarbes Cedex, France
e-mail: vincent.wagner@enit.fr

E. Duc
Clermont Université, IFMA, UMR 6602, Institut Pascal, BP 10448, 63000 Clermont-Ferrand, France

tool wear study where are presented the tool damages during milling of Ti-1023. The last section points the relation between the cutting speed and the tool life.

## 2 Titanium alloy presentation

For all experiments completed in this study, the workpiece material is a Ti-1023 titanium alloy containing iron (2 % of weight), aluminum (3 % of weight), vanadium (10 % of weight), carbon (0,01 % of weight), and the presence of oxygen, hydrogen, and nitrogen. The titanium is a structural $\beta$ titanium alloy and presents some interests for applications such as landing gears. The $\beta$-alloys compared to $\alpha - \beta$ alloys exhibit higher strength to density values and good strength-toughness combinations. In order to make tests in a homogenous material, the superficial coat has been removed.

The material composition of titanium alloys modifies the phase volume fraction with the phase stability. The titanium alloys can be divided in three categories:

- The quasi-$\alpha$ where the stable $\beta$ phase is very low (less of 5 %),
- the $\alpha + \beta$ alloys where the $\beta$ phase represent 5 to 10 % of the volume,
- the $\beta$ alloys,
- the quasi-$\beta$ where the $\alpha$ phase is very low.

This classification can be made according to $Al_{eq}$ and $Mo_{eq}$ which are the equivalent in aluminum and molybdenum of $\alpha$ and $\beta$ phases. They are respectively defined with the (1) and (2).

$$Al_{eq} = Al\%m + \frac{Sn\%m}{3} + \frac{Zr\%m}{6} + 10 \times (O_2\%m + C\%m + 2N\%m) \quad (1)$$

$$Mo_{eq} = Mo\%m + 1.5V\%m + \frac{Cr\%m}{0.6} + D\frac{Fe\%m}{3.5} + \frac{Cu\%m}{1,3} + \frac{Nb\%m}{3.6} \quad (2)$$

As described by [7], the type of titanium alloy can be defined based on a graph (Fig. 1).

The mechanical properties of the Ti-1023 are partially explained with its composition. The aluminum is an alphagene component which increases the alloy's hardness, the mechanical, and the fatigue resistance. However, this element affects its ductility. At room temperature, the iron increases the mechanical resistance, the ductility, and the creep. The component with the highest concentration, the vanadium, is a betagene element increasing the ductility but raises the corrosion alloy resistance. Its low density

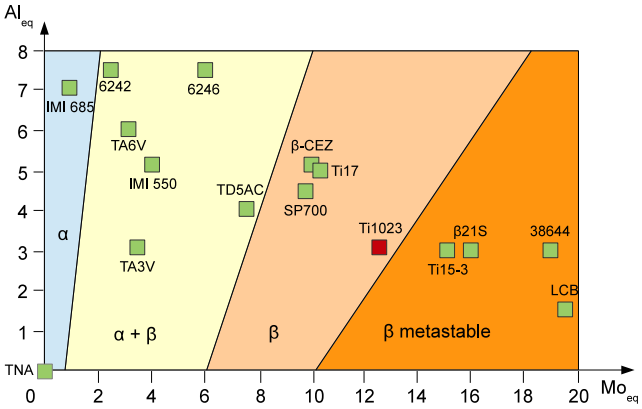


**Fig. 1** Type of titanium alloy according to $Al_{eq}$ and $Mo_{eq}$

combined with its good mechanical properties, the toughness and the fatigue resistance are the main causes of the Ti-1023 alloy use for the critical parts on airplane. The beta transus temperature is approximately 800 °C, the Ti-1023 alloy presents a better forgeability compare to the Ti-64 where the beta transus temperature is approximately 1830 °C.

Concerning the alloys used in this study, a first forging operation is carried out beyond 800 °C and a second forging operation is made under the beta-transus temperature (750 °C). The alloy properties improve its sensibility to heat treatments. In order to verify the alloy, a micrography has been carried out. A sample has been removed, embedded in a resin and a chemical etching (Kroll) has been made. With this forging process, the titanium alloy microstructure observed is a regular microstructure. It's divided in a primary $\alpha$ phase and a matrix which is composed of $\beta$ phase stabilized by the precipitations of secondary phase $\alpha$ (Fig. 2).

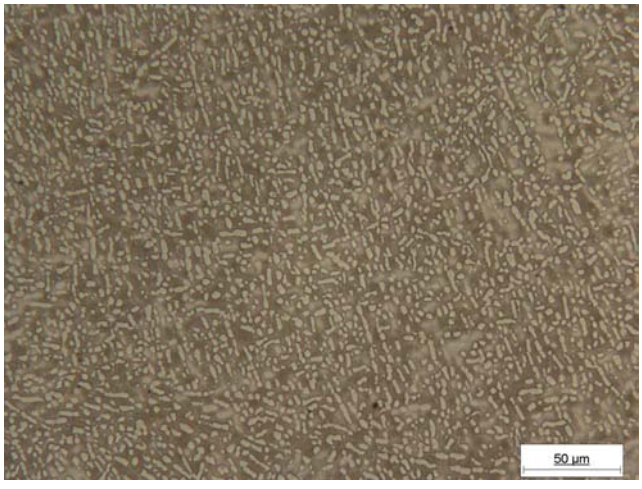


**Fig. 2** Ti1023 microstructure

**Table 1** Tools geometry and grade of tools

| Description | Tool 1 | Tool 2 |
|---|---|---|
| Commercial nuance | ST40 | CTC5240 |
| Coating | TiCn-Al2O3-TiN (CVD) | TiN-TiB2 (CVD) |
| Substrate | CW + Cobalt 21% | CW + Cobalt 10 % |
| Insert rake angle | 10 °C | 10–20 °C |
| Edge preparation | Honing 0.06 mm | Honing 0.07 mm |

## 3 Experimental setup

Some contouring operations were carried out using two tool holders and two different inserts. The cutting tool geometry and the type of grade are presented in Table 1. Concerning the tool 1, the reference of tool holder is R300-032A25-12H with a HSK63 attachment and the insert used is R300-1204E-PL S40T. The cutting tool geometry is defined in Table 2. For the tool 2, the tool holder reference is A251.40.R04.12RS with RPHX 1204M4EN M31 CTC 5240 inserts (Table 1).

Each insert has been embedded in a resin and cutted in order to measure the cutting tool geometry (Fig. 3). For both tool holders, the lead angle, the axial rake angle, and the index angle are equal to zero. Consequently, the axial rake angle and the radial rake angle are similar to the insert rake angle.

All tests have been carried out with external lubricant (Quakercool 8 %) and with low pressure (<12 bars). The three cutting force components were measured using a KISTLER quartz three-components dynamometer type 9257B and PC-based force acquisition system using Pimento software. The precision of acquisition was evaluated to be able to measure cutting forces with an error inferior to 3.5 %. The dynamometer was mounted on a numerical controlled milling device Huron KX15. The cutting power was measured with Siemens system, and they were treated with Matlab software.

The forces recorded by the dynamometer are represented as shown in Fig. 4. For a point of the tool cutting edge, $F$ is the resultant cutting forces with its three components: $F_a$, $F_r$, and $F_t$. $F_a$ is the axial force, $F_r$ is the radial force, and $F_t$ is the tangential force. The wear of the inserts was measured with a multi-sensor device Werth at regular intervals by interrupting machining operations.

## 4 Cutting conditions definitions

In industry, a practical method used to characterize the machinability of a particular couple of tool-material is to use the specific cutting energy ($W_c$). This method is presented in the next section. It shows the ratio between the cutting process in considering the cutting power and the material removal rate (3).

$$W_c = \frac{P}{Q} = \frac{P}{a_e a_e V_f} \tag{3}$$

where $P$ is the cutting power (W), $Q$ is the material removal rate (mm$^3$/min), $a_e$ is the radial depth (mm), $a_p$ is the axial depth (mm), and $V_f$ is the feed (mm/min).

Cutting power can be defined according two methods. The first is the measurement of the spindle power using a wattmeter [8]. The second method consists to use a dynamometer platform where the cutting power is calculated by the following relation (4):

$$P = \vec{F} . \vec{v} \tag{4}$$

with $\vec{F}$ : the cutting forces (N) and $\vec{v}$ : the velocity (m/s).

According to some observations made by [8], Deshayes and coworkers note a better definition of the cutting parameters in using dynamometer platform allowing to exclude cinematic effects of lathe [9]. The specific cutting forces and consequently spindle power remain stable over a range of cutting speed contrary to the power measurements.

Deshayes and coworkers compare the energies formulas for cutting power, specific cutting energy, and specific cutting force in oblique turning [9]. However, for milling

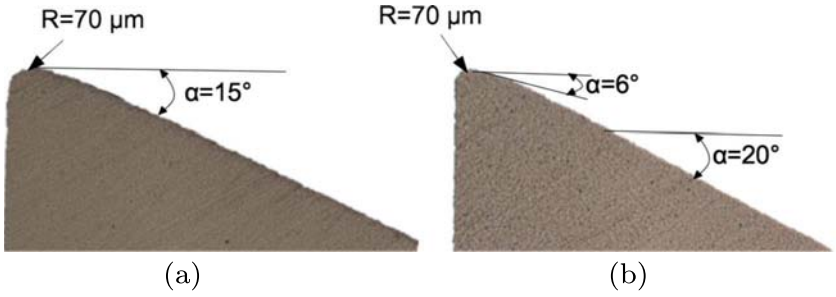


**Fig. 3** Cutting tool geometry for the tool 1 (**a**) and the tool 2 (**b**)

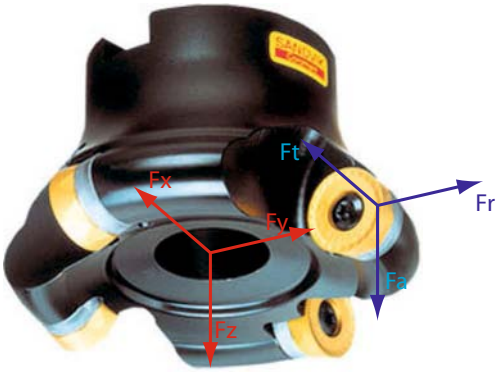


**Fig. 4** Cutting forces representation

operations, the cutting forces depend on the tool insert position. In this study, all cutting energies will be calculated according to the maximum cutting forces (5).

$$\begin{aligned} W &= FV_c \\ W_c &= F_c V_c t \\ Wr &= F_r V_f t \\ W_a &= F_a V_c t \end{aligned} \tag{5}$$

In using a toroidal cutter, the instantaneous chip cross-section depends of insert angular position, axial depth, insert radius, and axial depth of cut. Contrary to the contouring operations with cylindrical tool where the instantaneous chip cross section varies with the angular insert position and the feed. In order to define a model of cutting forces, [5] bases his model on the average chip thickness calculated by the following relations (6, 7, 8).

$$e_{moy}(\theta) = \frac{f_z sin(\theta) a_p}{r\left(\frac{\pi}{2} - asin\left(\frac{r-a_p}{r}\right)\right)} \tag{6}$$

$$e_{moy}(\theta) = \frac{f_z sin(\theta) a_p}{r\left(\frac{\pi}{2} - \varphi_0\right)} \, avec\, \varphi = asin\left(\frac{r-a_p}{r}\right) \tag{7}$$

$$e_{moy}(\theta) = \frac{f_z sin(\theta) a_p}{r\left(\frac{\pi}{2} - asin\left(\frac{r-a_p}{r}\right)\right)} \tag{8}$$

where $f_z$ is the feed rate (mm/tooth), $a_p$ is the axial depth (mm), $r$ is tool radius (mm), and $\theta$ is the insert position (°C)

However, this method does not allow to define the specific pressure for each insert position. For this study, the chip thickness will be defined with the following relation (9).

$$e(\theta) = \int_{\varphi_o}^{\frac{\pi}{2}} f_z sin(\theta) cos(\varphi) r d\varphi \tag{9}$$

### 4.1 Cutting speed influence

Figure 6 shows the specific cutting energies ($W$) for both tools. In first, whatever the cutting speed, the specific cutting energy for the tool 2 is the highest. The cutting tool geometry for the second tool is the sharpest. Consequently, there is a better tool penetration into the workpiece material and the cutting forces are reduced.

Concerning the evolution of the specific cutting energy for both tools, the influence of cutting speed is very low. For the tool 1, the specific cutting energies remain stable. The second tool's values is also stable when $Vc < 50\,m/min$. Once this value passed, the specific cutting energy increases

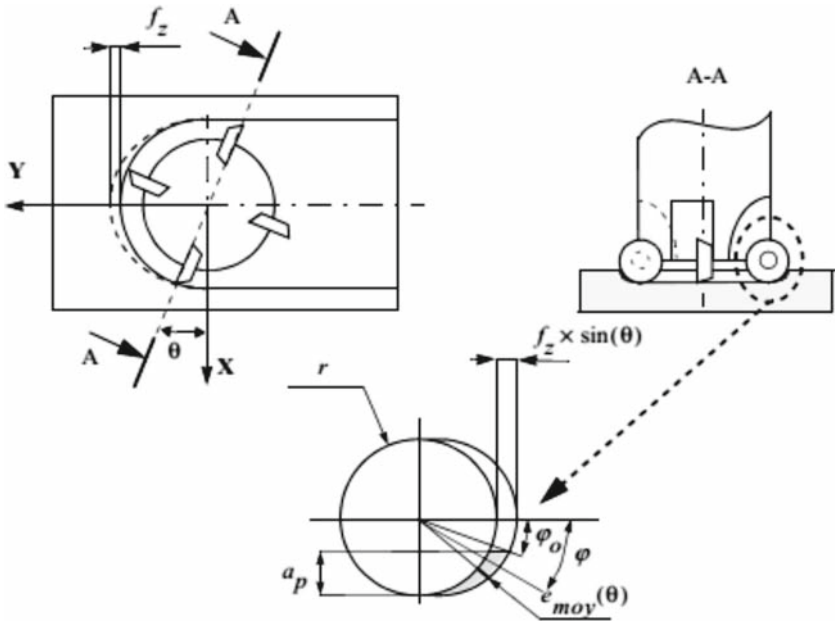


**Fig. 5** Geometry and parameters used for uncut chip cross section [5]

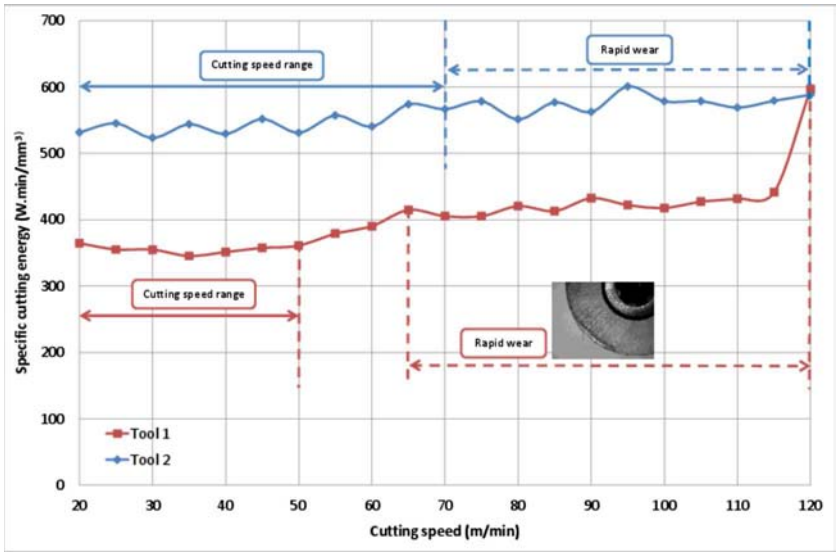


**Fig. 6** Evolution of specific cutting energy according to cutting speed

linearly until $V_c = 115\,m/min$. The highest value appears when $V_c = 120\,m/min$.

Based on the standard of the couple tool material, the range of an optimal cutting speeds is defined between two limits called $V_{cmin}$ and $V_{cmax}$. The lowest cutting speed named $V_{cmin}$ corresponds to the bottom limit. It's defined as the cutting speed where the specific energy remains minimum and with a minimum variation. For Ti-1023 machining and as for other titanium alloy [10], it's very difficult to define this limit. Concerning the tool 1, the $V_{cmin}$ appears when $V_c = 35\,m/min$ and for tool 2 the $V_{cmin}$ can be defined at $30\,m/min$. The maximal cutting speed ($V_{cmax}$) corresponds to the maximum cutting speed admissible by the tool. Generally, it's defined as the cutting speed where the tool wear becomes uncontrollable. When the cutting speed is higher than $V_{cmax}$, the specific energy is not considered as constant. Between the two limits, the process behavior must be controlled in different points. The tool life must have a physical and measurable value. The tool does not have a significant wear or a non-expected wear behavior. The disturbance phenomena such as chattering, dynamic tool deflections, or other machine tools dynamics phenomenon must be limited. In this case, the $V_{cmax}$ is defined when some tool wear appear. Concerning tool 1, the upper limit is $V_{cmax} = 65\,m/min$ and $V_{cmax} = 70\,m/min$ for the tool 2.

The evolution of the specific energy according to the cutting speeds observed for conventional material [8] does not appear clearly with some specific alloys. Indeed, the increase of cutting speed reduces the cutting forces with the thermal softening. Consequently, the specific cutting energy decreases. However, during the machining of Ti-1023, this evolution does not appear. Wagner and coworkers show also a low influence of cutting speed on specific cutting energy during the Ti-5553 machining [10]. These phenomena are explained by the high mechanical properties of titanium alloys in high temperatures combined with the low thermal properties of titanium alloys. They are often used for the rotating parts of aeronautical engine where the temperatures are high and where they must keep their mechanical properties. Moreover, the low thermal properties of titanium alloys compared to the cutting tool material restrict the temperature diffusion into workpiece material [1]. Consequently, the cutting temperatures during titanium alloys machining are very high but a major proportion of the thermal energy is transferred into the tool. The thermal energy is then too low to get the thermal softening as observed in traditional material. In order to get this thermal softening, some machining tests have been made in hot workpiece [11]. The tests show a low reduction of cutting force when the workpiece temperature is equal to 750 °C. These tests point the high strength of titanium alloys in high temperatures. Moreover, the high temperatures conducted into the tool promote the diffusion and consequently the tool wear. In order to get this thermal effect, some tests with highest cutting speeds can be made. However, the rapid tool wear observed when the cutting speed is among 65 and 120 m/min prevent these tests.

The specific cutting energies observed for the Ti-1023 alloy machining are often very high compared to the traditional materials and confirms its poor machinability. These observations corroborate with the conclusions form [12] and [13] which note that the $\beta$-titanium alloys are the most difficult to machine among all titanium alloys. This low machinability is mainly to the mechanical, chemical, and physical properties of titanium alloys.

The specific cutting energies observed with tool 2 are always the highest. To explain these phenomena, there is a difference of coating, which can modify stresses at the tool

chip interface [14] and consequently the cutting forces. The technique of coating deposit can also influence the roughness [15]. A rough surface leads to high frictions and may override the coating performance. As shown previously, the cutting tool geometry and especially the rake angle of the both tools is different and can induce some highest cutting forces.

Concerning the Ti-5553 dry turning [2] and for steel machining [16], some works show the influence of the cutting edge radius and the influence of the rake angle on cutting forces. The first study on the effects of cutting edge radius is made by Albrecht [17]. He states the presence of a stagnation point located below the cutting edge radius. This point is the limit where the workpiece material is divided into the chip and into the final part. Based on an experimental study, Albrecht concludes that the phenomena at the tool chip interface and under the edge radius are independent. When the cutting speed increases, the edge radius effect decreases due to a reduction of the built-up edge. However, the cutting edge radius can be a major part of the cutting forces especially when the uncut chip thickness is lower than the cutting edge radius. As described in Fig. 7, the stagnation point is located at $h_s$ . This height was studied attentively because the most of models concerning the effect of the edge radius are based on this height. In milling, Vogler and coworkers study the chip formation during milling with a frequency analysis [18]. They note a lower frequency compared to teeth excitation when the uncut chip thickness is lower to $h_s$, and they conclude that this frequency is due to the chip formation. In first, the workpiece material is upset until the uncut chip thickness is enough to form a chip. Accordingly, there is an higher cutting force and at a lower frequency. This difference is due to a better edge penetration in the workpiece material. A high rake angle generates also an increasing of the shear angle as illustrated by the model of [19]. During these tests, the highest rake angle is observed on the second tool. But, the angle at the vicinity of the cutting edge is very low. The effect of edge honed on cutting forces is then non negligible. Concerning the Ti-5553

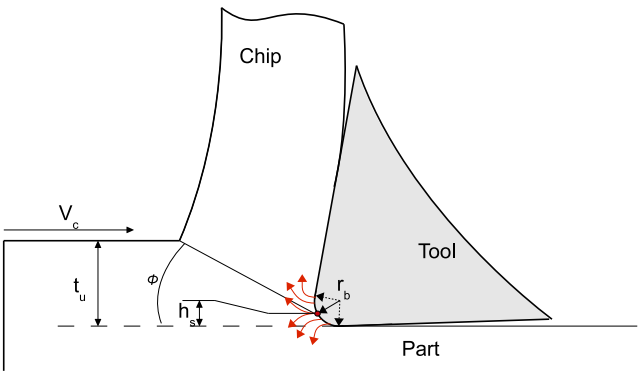


**Fig. 7** Influence of the cutting edge radius on cutting process

turning and based on the model developed by [20], Wagner states the influence of the honed cutting edge on the cutting forces [2]. He observes an increasing of cutting forces according to the cutting edge radius. This effect is amplified when the uncut chip thickness is lower than the cutting edge radius and its effect is reduced when the uncut chip thickness is two time the cutting edge radius. Moreover, the cutting tool geometry for the second tool is composed of two rake angles ($\alpha = 6°$C and $\alpha = 15°$C). Consequently, the effect of cutting edge radius is also amplified by the low rake angle. Based on the analysis of the cutting tool geometry effect, it's possible to use the effective rake angle as defined by [21]. Indeed, these equations show the relation between the relative size of the undeformed chip thickness to the tool edge radius, the effective rake angle and the separation point between chip and final part. Consequently, for the same cutting edge radius, a decrease of the uncut chip thickness and effective rake angle reduce the average rake angle and the cutting forces increase.

### 4.2 The feed rate effect on cutting process

Based on the French standard [6], the range of feed rate can be defined with an identical method. The minimal feed rate ($f_{zmin}$) is characterized when the specific energy is at its lowest level and when the tool wear can be controlled. The maximal feed ($f_{zmax}$) is defined when the specific energy increases or when some disturbance phenomena occur. Figure 8 shows the evolution of specific cutting energies according to feed rate for two cutting speed ($V_c = 40$ and 60 m/min) in order to validate the low effect of cutting speed.

Concerning the tool 1, the specific cutting energy begins with the highest value and decreases with the feed rise. The range where $W_c$ is stabilized and where no disturbance phenomena appeared ranges from $f_z$ of 0.1 to 0.3 mm/tooth for both cutting speeds. The evolution of the specific cutting energy of the second tool is different. The values start smaller compared to the first tool and decreases from 0.075 to 0.125 mm/tooth. When $V_c = 40m/min$, the specific cutting energy is stabilized. But after 0.175*mm/tooth*, some vibrations appear and the tool wear cannot be controlled. If $V_c = 60$m/min, the specific cutting energy increases from a feed of 0.15 *mm/tooth* and decreases. The region where $W_c$ is stabilized ranges from $f_z$ of 0.1 to 0.125 *mm/tooth*.

The reduction of the specific cutting energy is due to an increase of the instantaneous uncut chip thickness. Indeed, when the feed rate is lower than the radius of the cutting edge, the edge radius also generates the chip and some high specific pressures are produced. In order to avoid this phenomenon, the minimum feed rate is often chosen as equal to the value of the edge radius when straight edge is used. However for toroidal tool, use a minimal feed rate

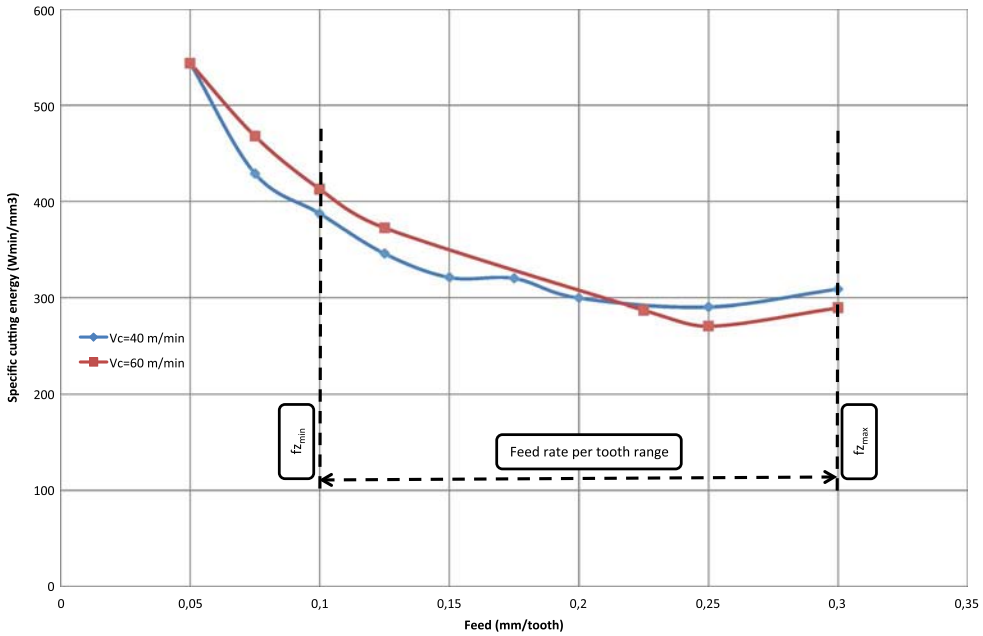


(a)

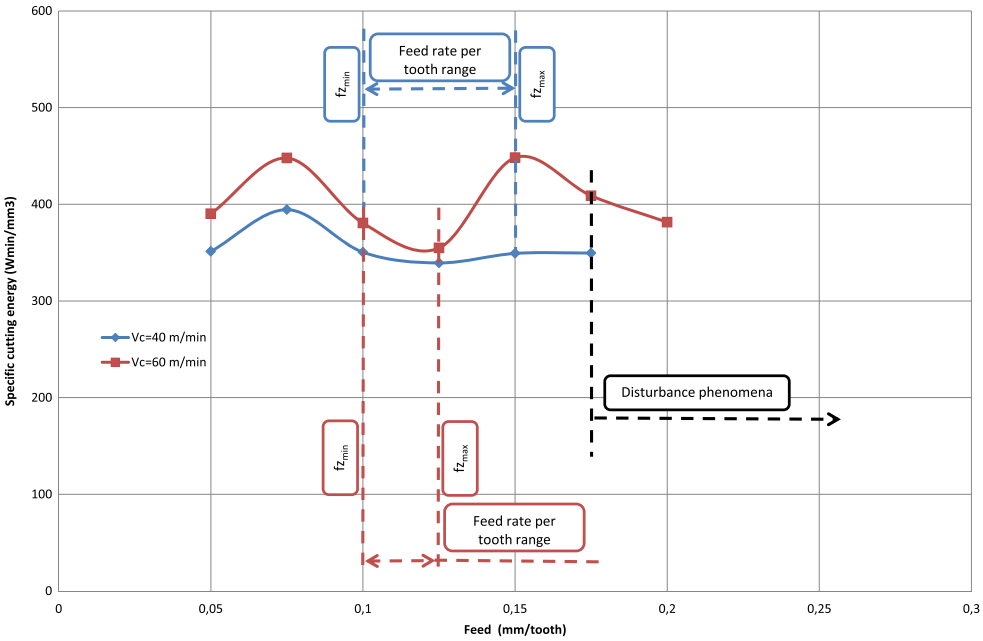


(b)

**Fig. 8** Evolution of specific pressure according to feed rate for tool 1 (**a**) and tool 2 (**b**)

equal to the edge radius is more difficult. Indeed, the uncut chip thickness is different along the edge. Figure 9 shows the evolution of the maximal uncut chip thickness at the vicinity of depth of cut according to axial and radial depth for an insert radius equal to 6 mm. When the radial and the axial depths decrease the maximal uncut chip thickness decreases.

For both tools, the uncut chip thickness is often smaller than the cutting edge radius. Consequently, the cutting edge radius effect is amplified. Moreover, the low rake angle at the vicinity of cutting edge for the second tool can increase the cutting forces.

### 4.3 Chip analysis

During machining tests, a difference in specific cutting pressure and consequently on the cutting forces has been observed. This is due to the cutting tool edge geometry (rake angle, rake angle close to the cutting edge, and the cutting tool edge radius). The cutting process generated by each

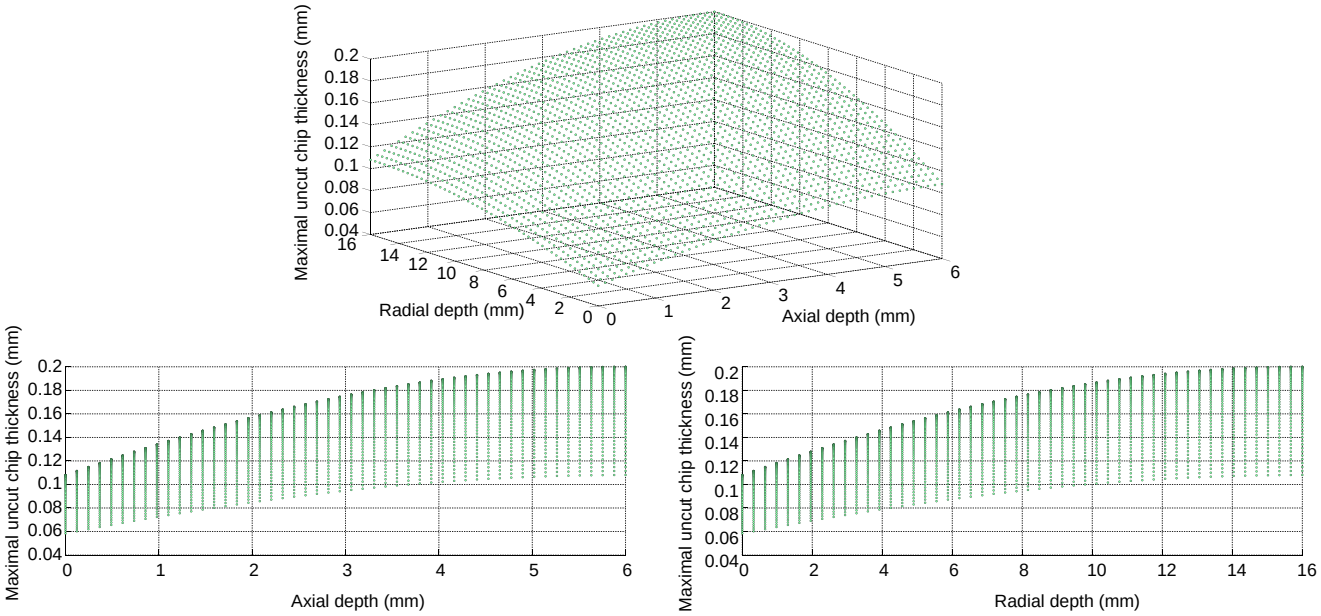


**Fig. 9** Evolution of uncut chip thickness for toroidal tool according to insert position and axial depth

tool and for each cutting condition can be also observed in analyzing the chip formation. This analysis is divided in two steps. The first step is the analysis of the chips morphology. The second level is the comparison of the chips microstructure obtained with different feeds and at several axial levels of chips. The state of the art is often focused on chip issues of turning operations where the uncut chip thickness does not depend of time. However, in milling and especially with a toroidal tool, the uncut chip thickness depends on insert angular position and axial depth. Consequently, each chip is analyzed in its totally length (total work period of insert) and for two levels ($a_p = 4$ and 2 mm). The first level corresponds to the highest uncut chip thickness a the top of the chip which is the limit of axial depth. In order to analyze the second level, each chip embedded in resin is polished to remove 2 mm of height.

Figure 10 shows the evolution of the chips morphology for different feeds. This study is focused on the chip obtained with the tool 2 because the same conclusions can be made with the first tool. In order to compare the different morphologies, each chip is compared to the theoretical chip. In first, the chip morphology is mainly influenced by the feed. When it is the lowest, the chip is the smallest and when the feed increases the recolted chip become similar at the theoretical chip. The second difference is the shape of each chip. For the lowest feeds ($f = 0.05$ and 0.1 mm/tooth), the chip seems to be totally wavy. Contrary to the chip obtained with the highest feed where the waves occur only at the bottom part of the chip. The second difference is observed at the free surface which is not in contact with the tool rake face. When the feed is $f = 0,05\,mm/tooth$, the surface is slight contrary to the chips generated with the highest feeds where some bands occurs.

The different chips morphologies can be explained with the analysis of the chip formation. As described previously, two cutting process which depend of feed, axial depth and insert radius, occur during machining with toroidal tools. The cutting process when the uncut chip thickness is lower than the cutting tool edge radius and the cutting process when the uncut chip thickness is higher than the cutting edge radius. These two cutting processes modify also the chip formation and the chip morphology. When the feed is the lower, the uncut chip thickness is always lower than the edge radius whatever the insert position and the axial position. The chip is formed only by plastic deformation and the chip is also wavy by the insert. These phenomena are amplified by the low chip thickness. The shear bands are also not observed on the free surface, which show the different chip formation. When the feed increases, the chip formation is also modified. The shear bands appear on the free surface of the chip. A study of chip microstructure was carried out on order to complete this analysis. To reveal the titanium alloy microstructure, a chemical attack has been made on each chip. As seen in the previous section, there is a relation between the feed and the chip microstructure and consequently with the chip formation.

Figure 11 shows the evolution of titanium alloy microstructure for several feeds and for two levels of the chip. When the feed is the lowest ($f = 0.05mm/tooth$), the shear bands don't appear clearly whatever the height analysed and the chip seems to be continuous. Consequently as described previously, the chip is mainly formed by plastic

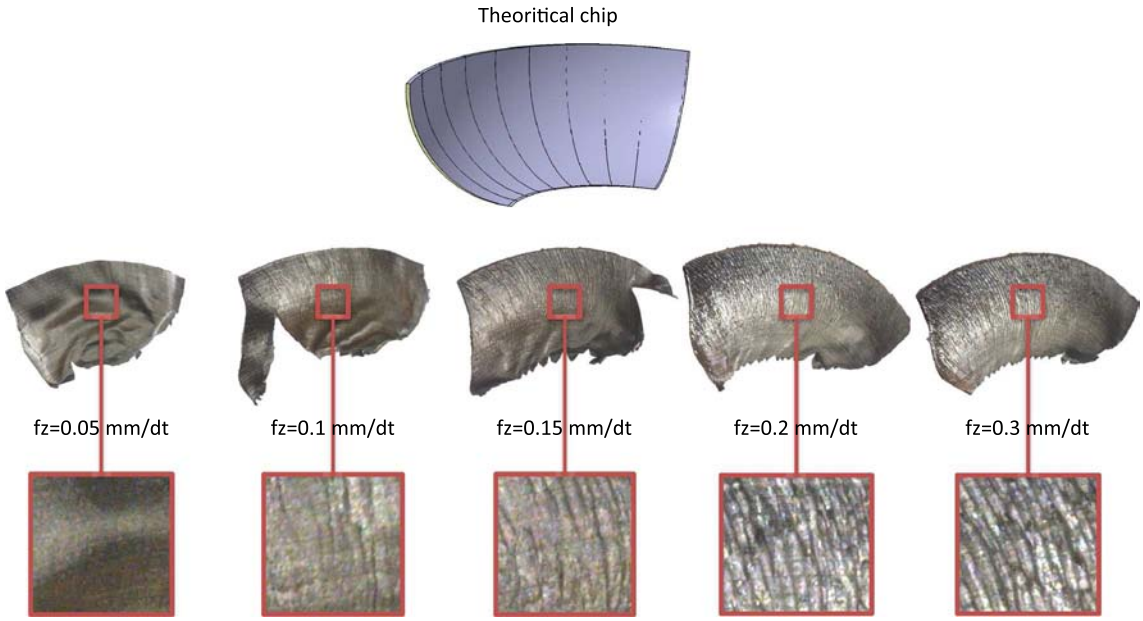


**Fig. 10** Evolution of chip morphology according feed

deformations and not by catastrophic shearing. The material is also ploughed by the cutting edge. When the feed increases, the chip formation is modified. Some shear bands appear especially when the uncut chip thickness is the highest (highest feed and highest $a_p$). According to [22], the transition from continuous to saw tooth chip formation is favored by the increase of the cutting speed, the undeformed chip thickness, and the decrease in the tool rake angle. For this analysis, these modifications occur directly on each chip at several angular positions and at several axial depths. When the feed increases, the uncut chip thickness becomes higher than the cutting tool edge radius and the chip formation changes. On a same chip, the type of chip can be different. When the insert comes into contact with the workpiece material, the uncut chip thickness is the highest. The chip is also a saw tooth chip. The uncut chip thickness reduces with the insert angular position and consequently the chip become continuous. The same conclusions can be made at a lowest axial depth but the transition between continuous chip and angular chip is modified.

The chips collected present some shear bands when the uncut chip thickness is the highest (Fig. 13a). All primary shear zones start at the chip base and with the same radius. This type of bands has been observed by [23]. The chip formation in machining of titanium alloys has been studied since many years. Several theories have been developed and discussed. The first is based on the theory of adiabatic shear catastrophic. During the cutting process, most of the deformation is concentrated in the primary shear plane. It appears a high rate of work hardening of the material. Moreover, most of the deformation energy is converted into heat energy. Consequently, there is a substantially increase of the temperature in the primary shear band. Due to this heat, the workpiece mechanical properties are then reduced. This phenomenon is called thermal softening. There is a catastrophic shear or adiabatic shear when the thermal softening effect exceeds the rate of hardening. According to the second theory, the segmented chip formation is the result of a crack initiation at the free surface and its spread to cutting edge in the primary shear plane. In their works, Poulachon and coworkers describe the chip formation for steel as four successive phases [24]. In despite of the number of models and of theories, the development of a new material with complex behavior, it is not always possible to predict phenomena and especially for the cutting process domain. Concerning the titanium machining, Komanduri explains the chip morphology in several steps [23]: (1) represents the undeformed surface of a chip. (2) is the $\alpha$ section of the primary shear plane. This zone is a part of the catastrophic shear zone, which is separated from the previous segment. (3) is the zone where an intense shear band is formed by catastrophic shearing during the failure stage of the segment formation. (4) is the zone in contact with the rake face where some intense shearing occurs. (5) is the primary shear plane where some intense localized deformations appear. As described by, the primary shear plane is curved. (6) is the machined surface.

When the uncut chip thickness is too low, this crack does not appear due to some low strains, stresses, and thermal effect (Fig. 13b).

The feed used must be a compromise in order to limit the effect of edge radius when the uncut chip thickness is

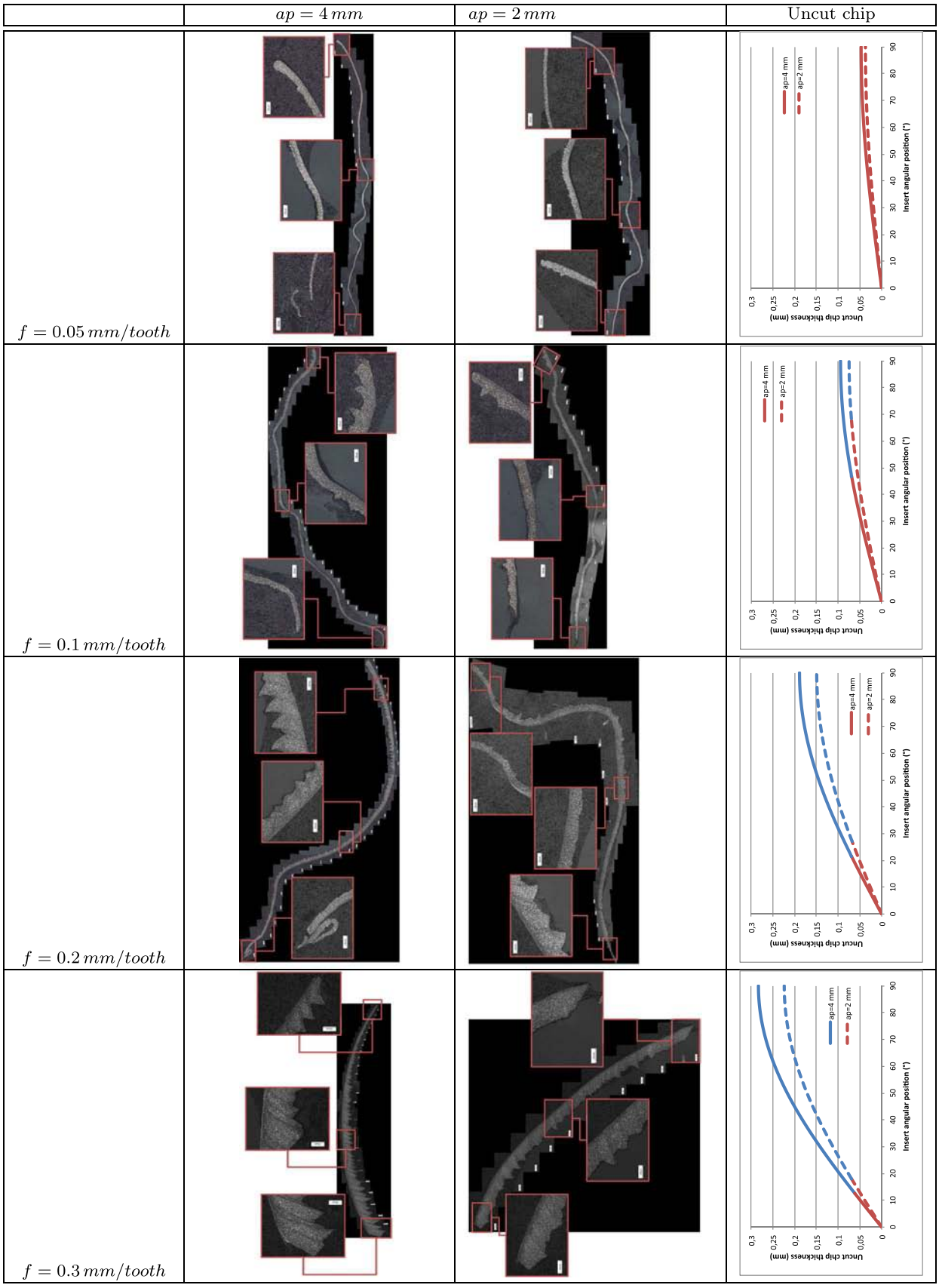


**Fig. 11** Evolution of chip formation for several feeds

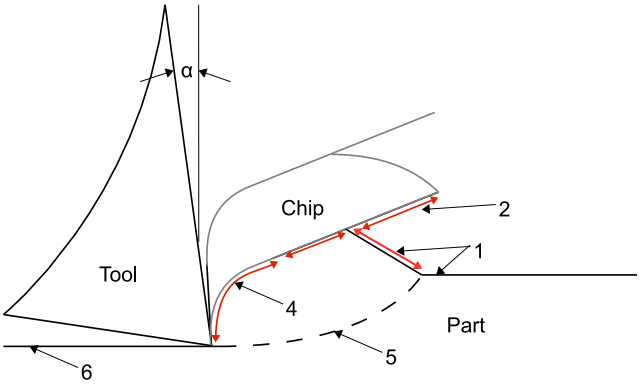


**Fig. 12** Chip formation during titanium machining ([23])

very low and to increase the effect of stress when the uncut chip thickness is high. However, the type of wear observed during these tests seems mainly due to some high frictions at the tool chip interface. Indeed, some edge failures occurred explain by the high stresses at the tool chip interface. The increase of feed generates an excessive uncut chip thickness and consequently some highest cutting forces and highest temperatures at the tool chip interface.

To conclude, it seems very difficult to define an optimal range of cutting conditions for Ti-1023 milling only based on workpiece behavior during machining. For example, the thermal energy provides by the cutting process is not enough to get thermal softening. This effect is amplified by the poor thermal conductivity of Ti-1023. The temperature is then evacuated into the tool and the cutting temperature is always too low in order to benefit thermal softening. Concerning the cutting speed tests, the minimal value has been defined for the lowest specific pressure for both tools. The maximal cutting speed will is defined according to the tool wear and no according to cutting process as defined in French Standard [6]. The specific pressure is stable, and the tool wear appears quickly. To conclude, the optimal cutting condition for Ti1023 is equal to conventional cutting speeds find in other titanium alloys ($35m/min < V_c < 80m/min$) [25].

## 5 Tool wear

This section presents the results of the tool wear study. The aim is the highlighting of the tool wear modes during the Ti-1023 milling with toroidal tool and the relationship between cutting conditions, tool life, and productivity. The Table 2 shows the evolution of the first tool after each test (150 mm). The second tool is presented Table 3.

### 5.1 Tool wear evolution

For both tools, the tool wear is divided in several steps. The first can be assimilated to a crater wear, which occurs like a concave section on the rake face generated by the chip sliding. The titanium machining is an abrasive process [10]. The contact between chip and tool on the rake face combined with high temperatures generates tearing of some coating particles. Concerning the Ti-64 turning, Corduan and coworkers observe a delimitation of coating into two layers before that coating is totally torn off [26]. They note a correlation between the cutting conditions and the tool failures. Freeman has studied the tool life of steel cutting grades (containing other material than tungsten) and straight WC/Co grades of cemented carbide in machining of two commercially available titanium alloys [27]. They show that plastic deformations occurred, especially for high cutting speeds and then shearing on rake face can form a crater. According to [4], some high frictions occur on the rake face of tool. Consequently, the heat is concentrated at the tool chip interface and the chemical reactivity of titanium generates some welding and accelerates the adhesion process.

The tool wear on the rake face during Ti1023 machining is located close to the main cutting edge. Moreover, its shape is similar to the uncut chip thickness (Fig. 14). Some marks appear on rake face in the direction of the chip flow angle.

Concerning the second step of the tool wear, a notch occurs always at the vicinity of the axial depth. According to [28], the side flow of the chip and the burrs on the workpiece was responsible of the formation of serious notch

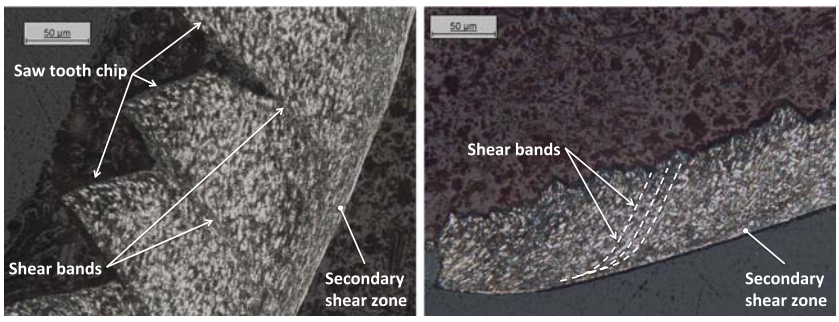


(a) (b)

**Fig. 13** Chip formation for the highest uncut chip thickness (**a**) and for the lowest uncut chip thickness (**b**)

**Table 2** Evolution of tool wear for Tool2 ($V_c = 60m/min$, $f_z = 0.3mm/tooth$, $a_e = 12.5mm$, $a_p = 4mm$)

| | | |
|---|---|---|
| Test 1 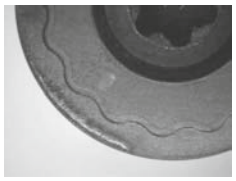 | Test 2 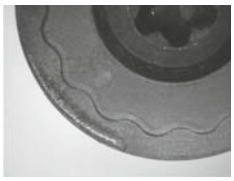 | Test 3  |
| Test 4 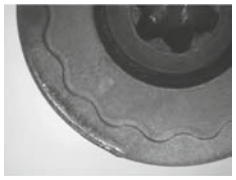 | Test 5 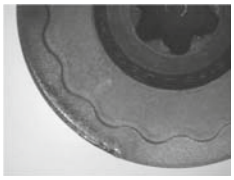 | Test 6 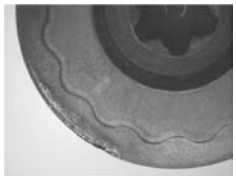 |
| Test 8  | Test 8 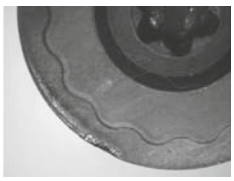 | Test 9 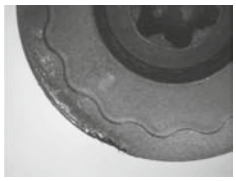 |
| Test 10 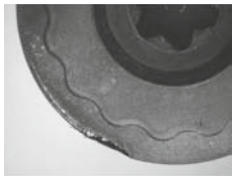 | Test 11 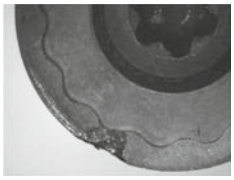 | |

wear. The notch is caused by a fracture process or a chemical reaction [29]. This type of tool wear is due too some high cutting temperatures on rake face explain by the mechanical and the thermal properties which lead to very high cutting temperatures (∼1000 °C. The hardness of the cutting tool materials decreases for high temperatures which aggravates the abrasive wear. For a toroidal tool, the maximum of cutting temperature occurs at the vicinity of axial depth where the uncut chip thickness is the highest. Moreover, the softer cutting edges due to the high temperature under the concentrated cutting forces near to the cutting edge and at the limit of axial depth generate some deflections and deformations.

**Table 3** Evolution of tool wear for Tool 1 ($V_c = 60\,m/min$, $f_z = 0.2\,mm/tooth$, $a_e = 12.5\,mm$, $a_p = 4\,mm$)

| | | |
|---|---|---|
| Test 1 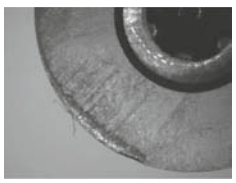 | Test 2 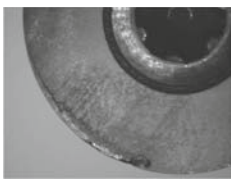 | Test 3 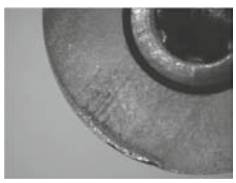 |
| Test 4 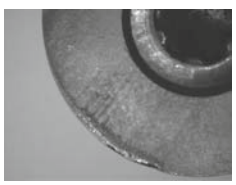 | Test 5 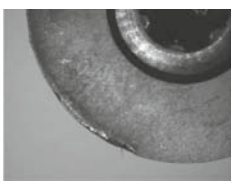 | Test 6 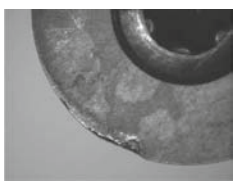 |

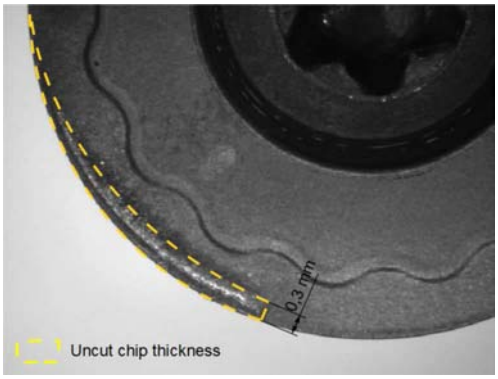


**Fig. 14** Tool wear pattern and instantaneous uncut chip thickness

The last cause is the intermittent milling process, which generate mechanical impacts and thermal shocks.

In order to verify the notch position, some tests have been made with some different axial depths (Table 4). The notch is always generated at the vicinity of axial depth where the uncut chip thickness is the highest. The reduction of axial depth leads to lowest uncut chip thickness and consequently lowest cutting forces and temperatures.

The control of the tool wear can be carried out according to classical tool wear criteria (Fig. 15). Several parameters on the flank face or on the rake face can be considered. The flank wear width which is measured in zone B in the cutting edge plane perpendicular to the main cutting edge. According to the standard [6], the width of the flank wear land is measured from the position of the original main cutting edge. However, the flank wear criteria, as $V_b = 0.3mm$, has never been reached. Indeed, the flank wear has been not observed during the tests. Concerning the rake face, the crater depth $KT$ is defined as the maximum distance between the crater bottom and the original face in region B (Fig. 15). However, an optical analysis has been made and during these test, this type of tool wear has not been observed. Moreover, the critical wear seems to be the notch wear for this configuration.

Figure 16 shows the evolution of the tool wear (crater width and notch width) and the spindle power according to the machining length. The notch wear and the crater wear were measured at their highest widths. As shown in Fig. 16, there is a correlation between the tool wear and the spindle power where two levels occur. Firstly, the power is stable and the value is between 2,000 and 1,900 W mainly due to a constant tool wear. After the ninth test, the power increases of 20 % and becomes stable around 2,200 W. The power evolution and notch width evolution are identical. The notch appears at the end of tool life and it is the critical factor to monitor the tool life. These tests point the low influence of crater wear on cutting process on the contrary to the notch wear that seems to be more influential. The increasing of cutting power is due to a modification of cutting tool geometry (rake angle). Moreover, the highest modification is located at maximal uncut chip thickness and its effect is then amplified.

The notch wear occurs also in flank wear but its effect on cutting power is not negligible. The tool will be then considered as worn when notch width exceeds 0.3 mm.

To summarize, the first damage is a crater wear close to the cutting edge where the coating is turn off. This stage represents 40 % of the total tool life. The cutting geometry is also damaged but the cutting process seems to be stable. However, the coating is turn off and the tool seems to be less resistant. A notch appears at the limit of axial depth where the crater width is the highest. The tool wear will be monitor with the notch width.

## 6 Cutting conditions influence on tool life and tool performance

This section presents the influence of the cutting conditions on tool life and tool performance.

Based on French standard or in Taylor's model, the tool life can be defined according to time (10).

$$a_p^F \left(\frac{a_e}{D_f}\right)^D f_z^E T^G V_c = C \tag{10}$$

But for the industrial, the productivity or the tool performance must be measured with material removal rate (11). It

**Table 4** Evolution of notch limit according to axial depth

| | $a_p = 2\,mm$ | $a_p = 4\,mm$ | $a_p = 6\,mm$ |
|---|---|---|---|
| | 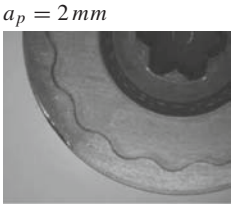 | 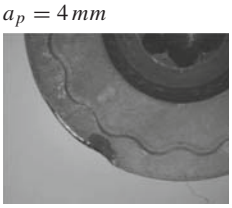 | 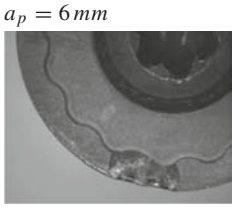 |
| Maximal uncut chip thickness (mm) | $0.15\,mm$ | $0.18\,mm$ | $0.2\,mm$ |
| Average uncut chip thickness (mm) ([5]) | $0.07\,mm$ | $0.10\,mm$ | $0.12\,mm$ |

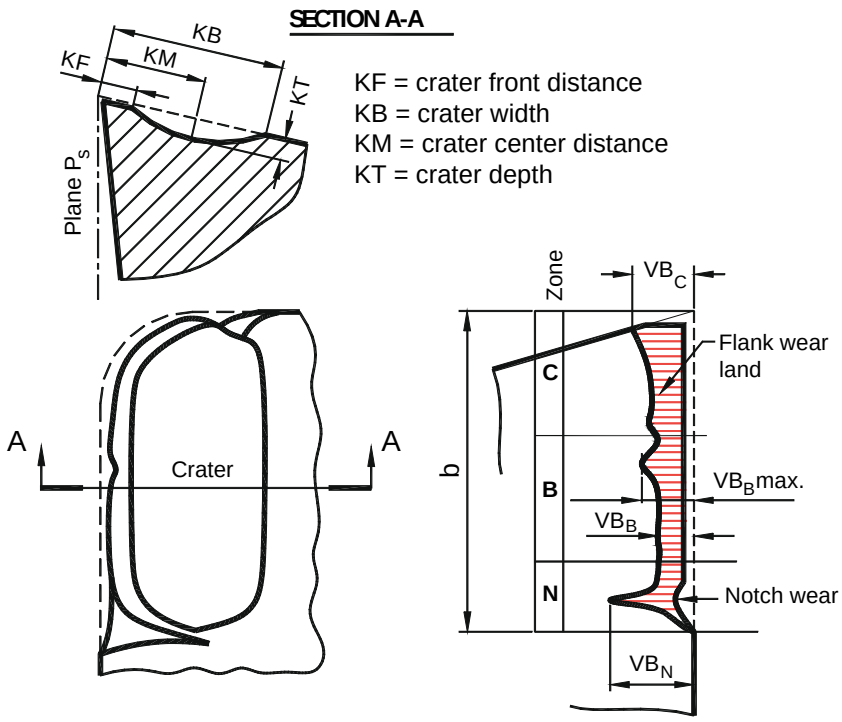


**Fig. 15** Tool wear criteria

is particularly important during roughing operations where the aim is to remove material in a short time.

$$Q = S\frac{1,000V_c}{\pi D}Zf_z \tag{11}$$

In order to link productivity and tool life, it seems important to use material removal rate combined to volume of material removed (V) (12).

$$V = SL \tag{12}$$

where $V$ is the volume ($mm^3$), $S$ is the cross chip section ($mm^2$), and $L$ is the length machined by one tool ($mm$).

### 6.1 Influence of cutting conditions

The analysis is made on four major axes : the tool life ($min$), the machining length ($mm$), the volume of material removed ($mm^3$) and the material removal rate ($mm^3/min$). Figure 17 show the evolution of the tool life in minute according to the cutting speed and the feed rate.

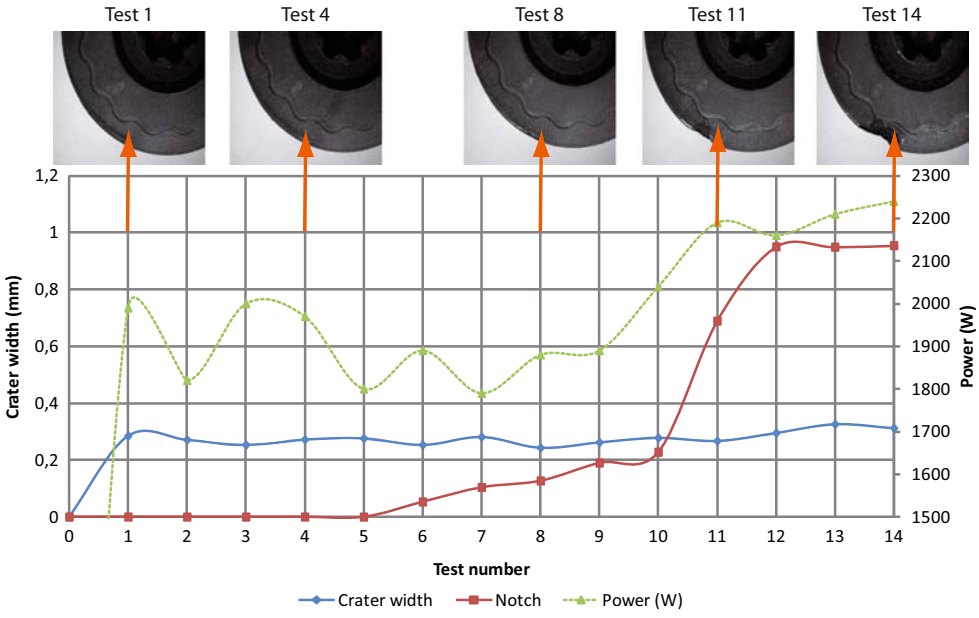


**Fig. 16** Evolution of tool wear, spindle power according to test number

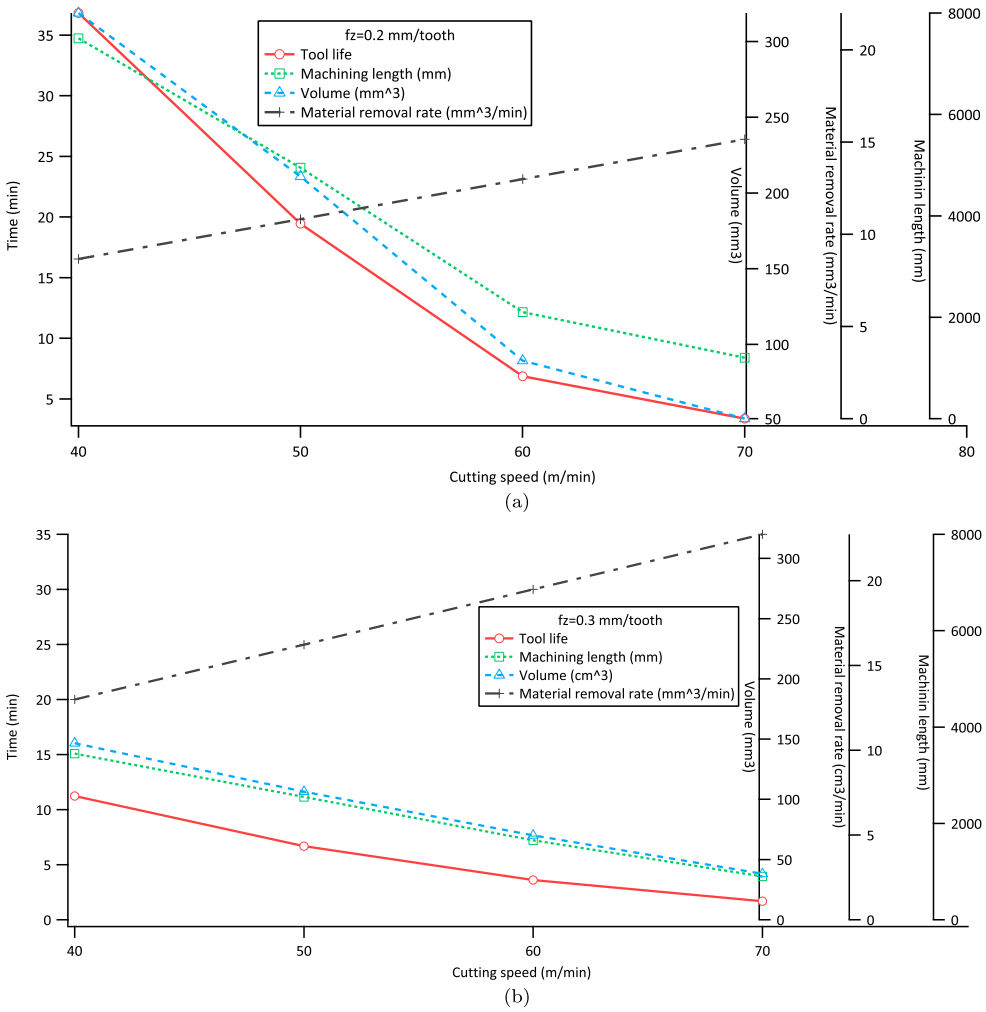


**Fig. 17** Influence of the cutting conditions on the tool life when $f_z = 0.2mm/tooth$ (**a**) and when $f_z = 0.3mm/tooth$

When the cutting speed increases, the tool life raises whatever the feed rate. However, the influence of the cutting speed on the tool life changes for the highest values ($Vc = 60$ and $70$ m/min). When $Vc = 60\,m/min$, the tool life attains 7 min and when feed is higher than $0.3mm/tooth$ the tool life decreases immediately (2 min when $f_z = 0.3mm/tooth$ and $V_c = 70m/min$). The same conclusions can be made for the machining length and for the volume. According to (12), the material removal rate increases linearly according to the cutting speeds.

As described in the previous section, the most influential parameter on the tool wear is the cutting speed. According to the analytical model from [19], an elevation of the cutting speed leads to an highest strain rate and an highest chip velocity. Accordingly, the cutting temperature at the tool chip-interface increases. With a thermocouple placed inside the tool close to the cutting edge, Wagner and coworkers observe the tool temperature [10]. They note an increase of the cutting temperatures with highest cutting speeds. Consequently, the tool life is affected by the cutting speed explains by the highest temperatures at the tool chip interface which induces the diffusion phenomena. There is a linear relation between the cutting forces and the uncut chip thickness. An increase of feed generates some highest cutting forces and some highest cutting temperatures and generates an highest diffusion. Moreover, the feed rate influences the mechanical impact between the insert and the workpiece material and may induce a shorter of tool life and generates some thermal cracks.

### 6.2 Influence of radial depth

The influence of the radial depth on the tool life has been also tested. The different works about titanium milling recommend several techniques to increase tool life. For example, the contouring operation must be made in down milling where the cutting tool is fed with the direction of rotation. In up milling, the tool is rotating at the opposite direction of the feed. Consequently, the instantaneous uncut chip thickness starts lower to increase to maximal uncut chip thickness. The edge radius mainly forms the chip and the cutting temperatures generate by rubbing may be

important. In down milling, the chip thickness starts bigger and a mechanical impact between insert and material occurs. However, this technic allows having a longer tool life because the cutting temperatures and the cutting forces are reduced. Several tool manufacturers purpose to use a radial depth lower than 30 % of tool radius generating a reduction of engagement curve. But the relation between radial depth and tool life for Ti-1023 milling with toroidal tool is still unknown. Some tests were performed with four radial depths ($ae = 8.5$, 12.5, 17.5, and 25 mm). Figure 18 shows the influence of radial depth in tool life and tool performances. An increasing of radial depth reduces the tool life and the cutting length while radial depth is lower than the tool radius (12.5 mm). For the highest values, the same tool life could be achieved (T=5.4 min). The difference appears especially in volume and in material removal rate. The volume increases with the rising of radial depth. This difference is explained by the highest cross section with highest radial depth ($a_e = 8.5\ mm$: $S = 42.5\ mm^2$; $a_e = 12.5\ mm$ : $S = 42.5\ mm^2$; $a_e = 17\ mm$ : $S = 60.5\ mm^2$; $a_e = 25\ mm$ : $S = 60.5\ mm^2$). In considering only the tool life, the best condition is $ae = 8.5\ mm$ where the highest values are observed. However, in the tool performance viewpoint, the better condition is $ae = 25mm$. In this case, a maximal volume is removed and with the highest material removal rate.

The better performance of tool when radial depth of cut is higher than tool radius is due to the evolution of cross chip section. However, an highest radial depth can modify the cutting process and explained the identical tool life gotten with $ae = 17$ and 25 mm. In milling operation, a cyclic variation due to the interrupted cutting generates some stresses and temperatures. A relation between thermal crack apparition and the cyclical variations of the cutting temperature in milling is pointed by [30, 31]. The thermal cycle for a tool is defined for continuous and interrupted cutting (Fig. 19). The plot $a$ represents the cutting temperature

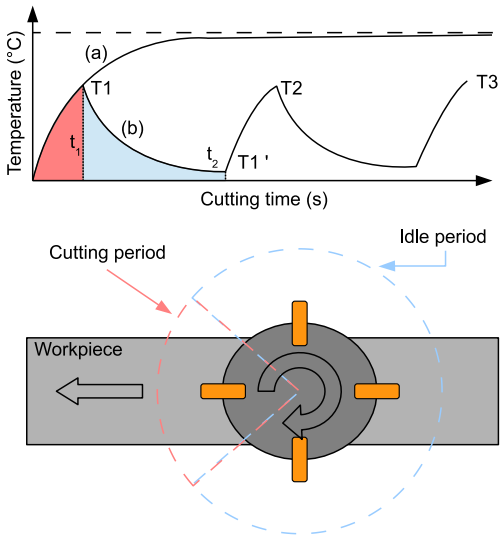


**Fig. 19** Cyclic variation during cutting temperature for interrupted and continuous cutting [30]

during continuous cutting where the temperature is rapidly stabilized. For interrupted cutting as milling operations, the curves are drastically different. During the cutting time $t1$ where cutting tool is in contact with the workpiece material, the tool heats to $T1$ temperature. The idle period begins at the end of $t1$ and, during the period $t2$, the tool cools to attain the temperature $T'1$ at the end of time $t1 + t2$. The total cycle is repeated for each insert revolution. For different materials, some metal cracks occur in tool and results of cyclic variations in stress and temperature [32]. The idle period and the cutting period are affected by the cutting conditions, the workpiece material, the tool material properties (thermal and mechanical properties), and the type of cooling (lubricant, air, and cryogenic system). According to [32], this cyclic variation of temperature causes the thermal cracking due to the very high chemical reactivity of titanium alloy, it has tendency to weld to the cutting tool during

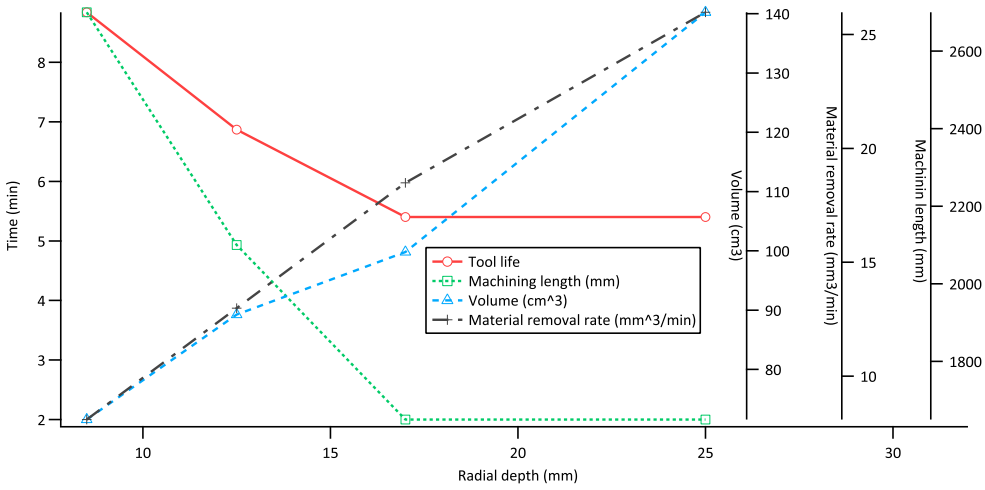


**Fig. 18** Influence of radial depth on tool life (Vc=70 m/min and fz=0,2 mm/dt)

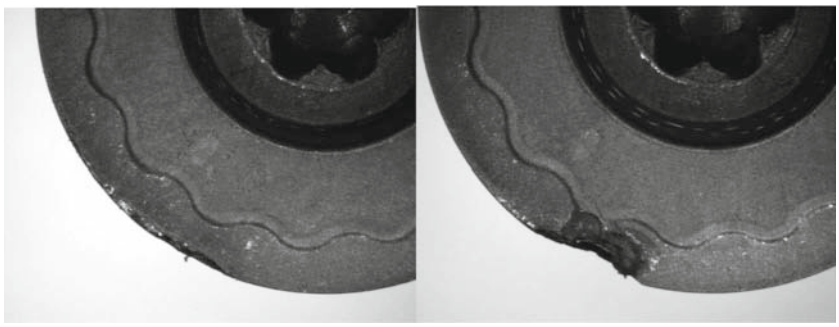


**Fig. 20** Evolution of tool wear when $ae < R$ (**a**) and when $ae > R$ (**b**)

machining which leads to chipping. This phenomenon is amplified with friction and high temperature near to cutting edge when insert penetrates the workpiece material.

In addition of this cyclic variation, some mechanical impact occurs between inserts and the workpiece material before each thermal and mechanical solicitation. The impact intensity is function of workpiece material, chip cross section but also function of the position of tool center compared to the machined surface. The relative position of tool modify also the length of cut and consequently the cutting and the idle periods. The last point noted by [2] is the impact position of tool edge.

Figure 20 represents the tool wear when radial depth is equal to 25 mm and when the radial depth is equal to 12.5 mm. The crater wear and the notch wear observed in the previous section do not appear. The tool wear is an edge chipping. Moreover, the spindle power measured when $a_e = 250$mm is between 1090 and 2020W. Compared to lower radial depth ($ae = 8.5mm$, $ae = 12.5mm$), the spindle power is stable in despite of number of teeth in material higher.

It appears that the most important influential phenomenon on the tool life is the impact between the insert and the workpiece. Its intensity is function of the workpiece material properties but also of the chip cross section. The position of tool according to machined surface can modify the impact intensity. To reduce it, then it is necessary to decrease the radial engagement and therefore the cutting section. The most unfavorable configuration is a radial depth equal to the tool radius. The impact is then the more important and where the cyclic variation of temperature is negative. The relationship between the tool life and the volume of material removed is not optimal in this case. If the radial depth is higher than the tool radius, the cyclic variation of temperature is damaging. Moreover, the contact is made on a portion of the insert very close to the cutting edge and which is not the machining section. Consequently, the impact and the solicitations which occur during the cutting period appear on two sections of cutting edge. The last case is a radial depth equal to the tool diameter. The energy of impact is then limits but the thermal solicitations are most important. Indeed, the idle time and the cutting time are also same. The cutting tool material is then weakened and some chippings appear.

### 6.3 Influence of axial depth

The last parameter tested is the axial depth (Fig. 21). In previous section, the notch position depends of axial depth. Moreover, the notch width is the lowest when axial depth

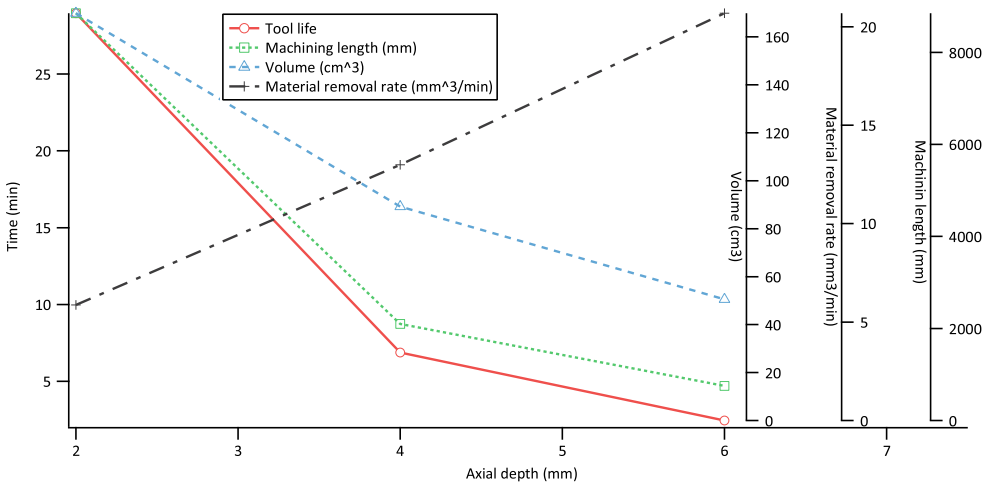


**Fig. 21** Evolution of volume and material removal rate according to axial depth

decreases. Compared to radial depth influence, a lowest axial depth expands the tool life. However, the gain of workpiece material removal rate is too low to grow the tool performance. Indeed, the volume decreases with an highest axial depth.

When axial depth decreases, the maximal uncut chip thickness is reduced. Consequently, the stresses and temperature on insert are lowest and the tool life rises.

## 7 Conclusion

This work presents a study of Ti-1023 milling with toroidal tool. In first section, the optimal cutting conditions for two tools have been defined. The tool material couple method describes in French standard has been used. The tests show a range of optimal cutting conditions in classical range find in common titanium machining. The chip formation and the chip morphology are also analyzed and show different phenomena on a same chip. In a second section, a tool wear analysis is made. The tool wear can be divided in two steps : a crater wear close to cutting edge and a notch wear at the axial depth limit. For industry, tool life is not the most important point. It seems important to define the best cutting condition and cutting engagement in order to increase productivity. Consequently, the last analysis is based on tool life but also material removal. Based on the results obtained in this works, the following conclusions can be drawn for milling:

- the relative position between the tool and the workpiece influences the tool life where the worst position is a radial depth equal to tool radius where impact between insert and workpiece is high and damage cutting edge appears,
- to increase tool life, the radial depth must be the lowest according to minimal uncut chip thickness,
- to raise the material removal rate, the radial depth must be highest than tool radius.

**Acknowledgments** The authors would like to express their thanks to Aubert & Duval for his support during this experimental work.

## References

1. Ezugwu E, Wang Z (1997) Titanium alloys and their machinability–a review. J Mat 68:262–274
2. Wagner V (2011) Improvment of machinabiltiy of refractory titanium: the ti-5553, Ph.D. thesis . University of Toulouse - France
3. Arrazola P, Garaya A, Iriartea L, Armendiaa M, Maryab S, LeMaitre F (2009) Machinability of titanium alloys (ti6al4v and ti555.3). J Mater Process Technol 209(5):2223–2230. doi:10.1016/j.jmatprotec.2008.06.020
4. Machai C, Biermann D (2011) Machining ob beta-titanium allloy ti-10v-2fe-3al under cryogenic conditions: cooling with carbon dioxide snow. J Mater Process Technol 211(6):1175–1183
5. Gilles P, Monies F, Rubio W (2007) Optimum orientation of a torus milling cutter: Method to balance the transversal cutting force. Int J Mach Tools Manuf 47(15):2263–2273
6. Working zones of cutting tools couple tool material part 1 general presentation, NF E 66-520-1
7. Combres Y Metallarugy and recyclability of titanium and its alloys, Technique de l'ingénieur.
8. Maitre FL (1980) Relations between cutting energies and tools damage. Wear 62:139–160
9. Deshayes L (2007) Analysis of an equivalent tool face for the cutting speed range prediction of complex grooved tools. J Mater Process Technol 190(1–3):251–262. doi:10.1016/j.jmatprotec.2007.02.037
10. Wagner V, Baili M, Dessein G, Lallement D (2011) Experimental study of coated carbide tools behaviour: Application for ti-5-5-5-3 turning. Int J Mach Mach Mater 9:233–248
11. Baili M, Wagner V, Dessein G, Sallabery J, Lal D (2011) An experimental investigation of hot machining with induction to improve ti-5553 machinability. Applied Mechanics and Materials 62:67–76
12. Donachie M (2004) A technical guide, 2nd edn., ASM, Ohio
13. Zlatin N, Field M (1973) Procedures and precautions in machining titanium alloys. Titan Sci Technol:489–504
14. Moufki A, Molinari A, Dudzinski D (1998) Modelling of orthogonal cutting with a temperature dependent friction law. J Mech Phys Solids 46(10):2103–2138. doi:10.1016/S0022-5096(98)00032-5
15. Padley S, Deevi S (2003) Single layer and multilayer wear resistant coating of (ti,al)n: a review. Mater Sci Eng A 342(1–2):58–79
16. Ranganath S, Campbell AB, Gorkiewicz DW (2007) A model to calibrate and predict forces in machining with honed cutting tools or inserts. Int J Mach Tools Manuf 47(5):820–840. doi:10.1016/j.ijmachtools.2006.06.019. Tehran International Congress on Manufacturing Engineering (TICME2005)
17. Albrecht P (1960) New developments in the theory of the metal-cutting process - part i. the ploughing process in metal cutting. ASME J Engg Ind 82:348–358
18. Kapoor MVRDS (2003) Microstructure-level force prediction model for micro-milling of multi-phase materials. ASME J Eng Ind 125(2):205–209
19. Oxley P (1989) Mechanics of machining: an analytical approach to assessing machinability, Ellis Horwood Limited(UK), 1989
20. Ren H, Altintas Y (2000) Mechanics of machining with chamfered tools. J Manuf Sci Eng 122(4):650–659. doi:10.1115/1.1286368
21. Manjunathaiah J, Endres W (2000) A study of apparent negative rake angle and its effect on shear angle during orthogonal cutting with edge radiused tools, Transactions-North american manufacturgin research institution of (2000). pp 197–202
22. Barry J, Byrne G (2002) The mechanisms of chip formation in machining hardened steels. ASME 124(3):528–535
23. Komanduri R, Von Turkovich B (1981) New observations on the mechanism of chip formation when machining titanium alloys. Wear 69(2):179–188
24. Poulachon G, Moisan A (1998) A contribution to the study of the cutting mechanisms during high speed machining of hardened steel. CIRP Ann Manuf Technol 47(1):73–76
25. Koning W (2005) Applied research on the machinability of titanium and its alloys. In: Proceedings of the institution of mechanical engineers part B: management and engineering manufacture, vol. 204. pp 53–60

26. Corduan V, Himbart T, Poulachon G, Dessoly M, Lambertin M, Vigneau J, Payoux B (2003) Wear mechanisms of new tool materials for ti-6ai-4v high performance machining. CIRP Ann Manuf Technol 52(1):73–76. doi:10.1016/S0007-8506(07)60534-4
27. Freeman R (1974) The machining of titanium and some of its alloys, Ph.D. Thesis. University of Birmingham, Birmingham
28. Kitagawa T, Kudo A, Maekawa K (1997) Temperature and wear of cutting tools in high speed machining of inconel 718 and ti-6al-6v-2sn. Wear 202(2):142–148
29. Turkes E, Orakes S, Neselie S, Yaldiz S (2011) Linear analysis of chatter vibration and stability for orthogonal cutting in turning. Inte Anal Chatter Vib Stab Orthogonal Cut Turning 29:163–169
30. Palmai Z (1987) Cutting temperature in intermittent cutting. Int J Mach Tools Manuf 27(2):261–274
31. Ferrasi D (1972) Metal cutting, Metalo Society
32. Trent E, Wright P (1986) Metal cutting, 2nd edn., vol. 2. Butterworth, London